JOURNAL OF MATERIALS SCIENCE 30 (1995) 3839–3846

Assessment of oxygen in silicon carbide fibres

D. UPADHYAYA, F. H. FROES
Institute for Materials and Advanced Processes, University of Idaho, Moscow, ID 83844, USA
J. F. WATTS
Department of Materials Science and Engineering, University of Surrey, Guildford, Surrey GU2 5XH, UK
C. M. WARD-CLOSE
Structural Materials Centre, DRA Farnborough, Hampshire GU14 6TD, UK, Hampshire

Five different types of SiC fibre produced by chemical vapour deposition were analysed using Auger electron spectroscopy (AES), scanning electron microscopy (SEM) and X-ray (WDX) analysis. Fibres studied include SCS0, SCS6, Sigma SM1240 and two types of SiC fibres denoted SAM1 and SAM2, produced in the Commonwealth of Independent States (Ukraine, former USSR). Fibres were fractured *in situ* in the Auger spectrometer. For each fibre, the oxygen, carbon and silicon yields were measured and qualitative assessment of oxygen was performed. Results suggest that the SCS0 fibre contains less oxygen than other SiC fibres. It was revealed that the SAM1 fibre (120 μm diameter) has a duplex SiC and carbon coating deposited over a 20 μm tungsten core prior to the main SiC deposition, to decouple mechanically the tungsten core from the main SiC deposition.

1. Introduction

Metal matrix composites (MMCs) have particular applications in aerospace where components are required to withstand much higher mechanical and thermal stresses than can be sustained by monolithic materials [1]. At present, two types of continuous silicon carbide fibre, the SCS series (Textron Specialty Materials, Lowell, MA, USA; SCS*i*; $i = 2, 6, 8, 9$) and Sigma (DRA Sigma, Defence Research Agency, Farnborough, UK; SM1240 and SM1140) are available in single-fibre form and enough data are available on these fibres for consideration as a reinforcement. However, generally, information is not available on continuous SiC fibres produced in the former USSR. This paper assesses the amount of oxygen present in each fibre and reports on fibres produced in the former USSR, denoted SAM1 and SAM2.

It has long been known that titanium forms extensive interstitial solutions with oxygen causing embrittlement. Further, silicon carbide reacts with oxygen at high temperatures because of the higher chemical affinity of silicon for oxygen than for carbon [2]. The partial pressure of oxygen plays an important role in the oxidation of SiC. At low partial pressures (0.1 atm), volatile SiO forms, while at high partial pressures passive oxidation occurs forming a layer of amorphous or crystalline SiO_2 on the surface [3]. Several other intermediate chemical reactions are also possible. During passive oxidation of polycrystalline SiC, oxygen diffuses through the oxide scale and along the grain boundaries, while CO and CO_2 diffuse in the opposite direction [2]. It has been suggested that passive oxidation followed by the grain-boundary diffusion may lead to significant changes in fracture toughness and strength of hot-pressed SiC [2]. Equations 1–4 show the free energy of formation for various reactions calculated using a CSIRO thermochemistry computer program [4]

$$2Si + O_2(g) = 2SiO \quad \Delta G_{1200\,K\ (1\ atm)} = -95.3\ \text{kcal mol}^{-1} \tag{1}$$

$$Si + O_2(g) = SiO_2 \quad \Delta G_{1200\,K\ (1\ atm)} = -166.3\ \text{kcal mol}^{-1} \tag{2}$$

$$Si + C = SiC \quad \Delta G_{1200\,K\ (1\ atm)} = -13.7\ \text{kcal mol}^{-1} \tag{3}$$

$$2SiC + 3.5O_2(g) = 2SiO_2 + CO(g) + CO_2(g)$$

$$\Delta G_{1200\,K\ (1\ atm)} = -451.2\ \text{kcal mol}^{-1} \tag{4}$$

Most previous work has concentrated on the SCS series fibres and limited data are available on Sigma fibres. The microstructure of SCS series and Sigma fibres will not be discussed here; detailed information can be found elsewhere [5–9]. The amount of oxygen as well as the consistency of the oxygen, from one fibre production batch to another, plays an important role in determining the long-term performance behaviour of MMCs, especially titanium matrix composites [10]. It is reported that in SCS6/IMI-829 (Ti–5.5Al–3.5Sn–3Zr–1Nb–0.25Mo–0.3Si) matrix composite the hardness of the matrix close to the fibre is increased compared to the bulk matrix. Diffusion of oxygen from the SCS6 fibre to the matrix was suggested as one of the

0022–2461

probable causes [11]. Another study suggested that the air atmosphere has a pronounced effect on the degradation of composite properties (embrittlement of interface) compared to vacuum [12]. Oxygen diffusion from the atmosphere and internal oxidation of the composite were reported to be the primary causes for the embrittlement of the interface. A similar conclusion was drawn for the reduction in the low-cycle fatigue life of SCS6/Ti–6Al–4V composite [13]. It is clear that the presence of oxygen has significant effects on the resulting composite properties.

Little information regarding the oxygen in SiC fibre is available for SCS6 fibre and there is no information on Sigma fibre. Das [11] reported, on the basis of Auger analysis of *in situ* fractured single SCS6 fibres, and in an IMI-829 matrix composite, that the fibre contains high levels of oxygen (10–14 at %) which vary across the diameter of the fibre [11]. However, one report on Auger and neutron activation analysis of SCS6 fibre suggested that the fibre contains no oxygen, except at the outer fibre surface [14]. Bulk oxygen determination via neutron activation analysis suggested 0.1 at % oxygen in the SCS6 fibre [14]. It is clear that more work is required. This study is the first concentrated effort to assess the presence of oxygen in SiC fibres produced with different process parameters, although using a common chemical vapour deposition (CVD) technique.

2. Experimental procedure

Five different types of single continuous silicon carbide fibres (see Table I) were fractured *in situ* in an Auger spectrometer under ultra high vacuum ($< 10^{-9}$ mbar) conditions. Auger spectra were taken from each type of fibre within 5 min of fibre fracture to eliminate any possibility of oxygen contamination of the fracture surfaces. Oxygen, silicon and carbon intensities of the AES spectra were measured using a peak-background algorithm and a qualitative assessment of oxygen was made for each fibre.

Auger electron spectroscopy was performed on a high-resolution VG Scientific MA500 scanning Auger microscope. An electron-beam energy of 15 keV inducing a specimen current of 25nA was used. The hemispherical sector electron energy analyser was operated in the constant retard ratio (CRR) mode of 4. Data were recorded on a Link Analytical AN10000 data system. All Auger data reported in this paper are in terms of raw Auger intensities. No effort has been made to quantify the spectra as this would require knowledge of Auger cross-section, backscattering factors, and other physical and instrumental parameters. However, all spectra were recorded under identical spectrometer conditions, thereby allowing direct comparison between them.

Scanning electron micrographs were acquired on a Cambridge S250 microscope. X-ray linescan/mapping techniques were used to characterize elemental distribution in each fibre. This was performed on an analytical/scanning electron microscope Jeol 8600, which has an eight crystal light element detector and a fully computerized image analysis system. For this work, a wavelength dispersive X-ray (WDX) system was used throughout.

For the preparation of SEM and WDX specimens, fibres were embedded in the Bakelite and fibre ends were mechanically polished progressing from 75 μm to 0.04 μm Al_2O_3 slurry, and polished surfaces were achieved.

3. Results and discussion

3.1. Fibre characterization

The SCS series fibres and Sigma fibres are produced by different processes, although both involve the chemical vapour deposition technique [15–17]. The SCS series fibres themselves differ mainly with respect to fibre diameter (e.g. SCS9 is 75 μm in diameter) and composition of the outermost protective coating [5]. The Sigma SM1240 and Sigma SM1140 fibres have different types of outer-most coating. The production process for SAM1 and SAM2 fibres is not known except that the SiC has been deposited by CVD.

Fig. 1a–e show scanning electron (SEI) and backscattered electron (BSE) images of different SiC fibres. A 20 μm tungsten substrate is used for the deposition of SiC for both the SAM1 and SAM2 fibres. The SAM1 fibre exhibits a ring-like structure. Higher magnification BSE image of this region is shown in Fig. 2. The coating adjacent to the tungsten core is approximately 2.5 μm thick. The Auger spectrum of this region consists of two main signals at 89 eV (Si *LVV*) and 270 eV (C *KLL*) indicating the presence of SiC. Oxygen (O *KLL* at 510 eV) is also present (Fig. 3a). The SiC coating is followed by a 1 μm thick carbon coating, as indicated in the Auger spectrum (Fig. 3b) from this region. Fig. 4a shows a schematic X-ray

TABLE I Description of various continuous silicon carbide fibres

Fibre	Acquistion source[a]	Fibre diameter (μm)	Core (diameter in μm)	Producer
SAM1	UAS, Kiev, Ukraine	120	W (20)	CIS (former USSR)
SAM2	UAS, Kiev, Ukraine	170	W (20)	CIS (former USSR)
SCS0	ONERA, Paris, France	139	C (33)	USA (Textron)
SCS6	DRA, Farnborough, UK	142	C (33)	USA (Textron)
Sigma SM1240	DRA, Farnborough, UK	100	W (14)	UK (DRA Sigma)

[a] UAS = Ukrainian Academy of Science (courtesy Dr P. Silenko); ONERA = Office National d'Etudes et de Recherches Aerospatiales (courtesy Dr A. Vassel); DRA = Defence Research Agency (courtesy Dr R. A. Shatwell).

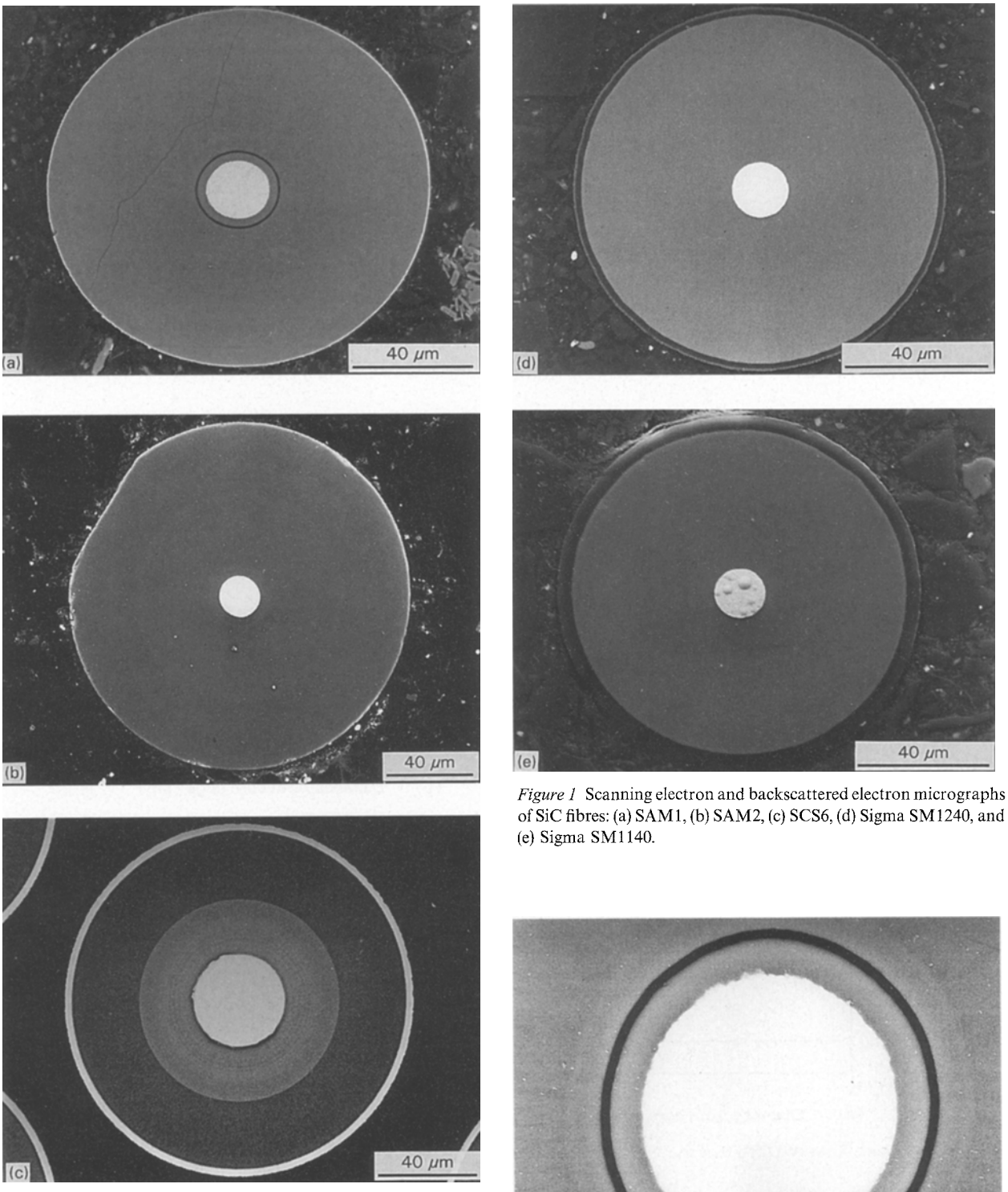

Figure 1 Scanning electron and backscattered electron micrographs of SiC fibres: (a) SAM1, (b) SAM2, (c) SCS6, (d) Sigma SM1240, and (e) Sigma SM1140.

Figure 2 Backscattered electron micrograph of the SiC/C coating region (near the tungsten core) of the SAM1 fibre.

(WDX) linescan of the distribution of silicon and carbon across the SAM1 fibre radius. The silicon concentration does not vary except in the carbon coating region and the carbon concentration increases in this region.

Similar observation can be made from the X-ray (WDX) elemental maps of this region, shown in Fig. 5. The reason for depositing silicon and carbon on the tungsten core in SAM1, prior to the main SiC deposition is not clear. It may be to decouple the core from the main SiC deposition and thus eliminate the detrimental effect of cracks originating from the SiC/W interface. To verify this, mechanical data are required; however, single-fibre tensile testing was not possible because of the limited availability of SAM1 fibres. The deposition of SiC prior to carbon coating seems reasonable. Carbon deposition over a hot tungsten substrate may result in extensive reactions between the tungsten core and the carbon deposit. This would cause either burning of the tungsten core or the formation of a significantly thicker reaction zone [18].

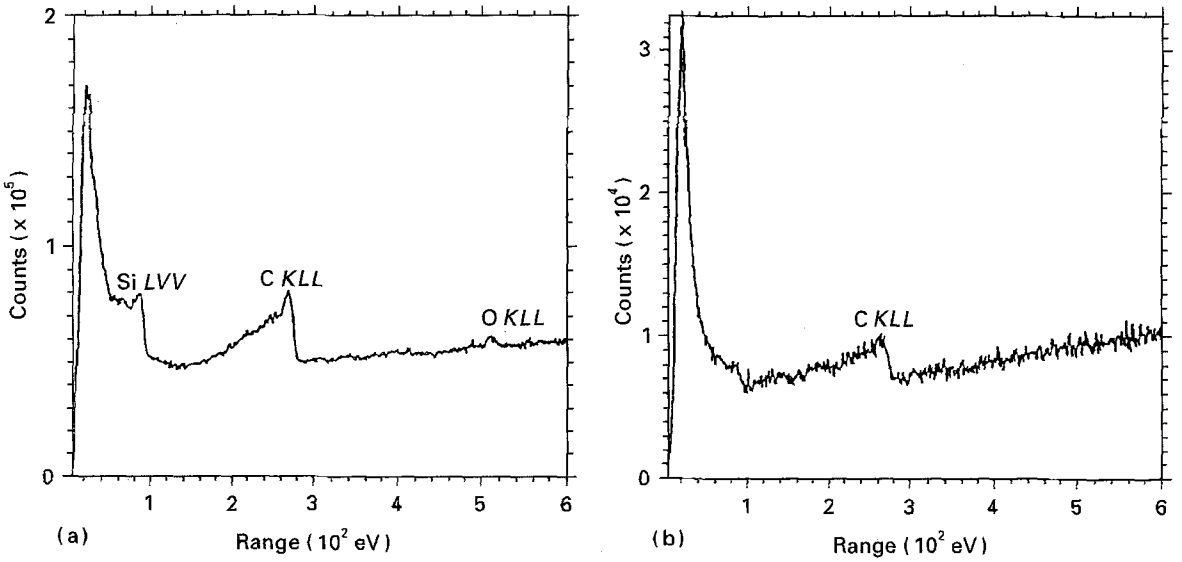

Figure 3 Auger point spectra of the SAM1 fibre from (a) the SiC coating near the tungsten core, and (b) the carbon coating near the tungsten core.

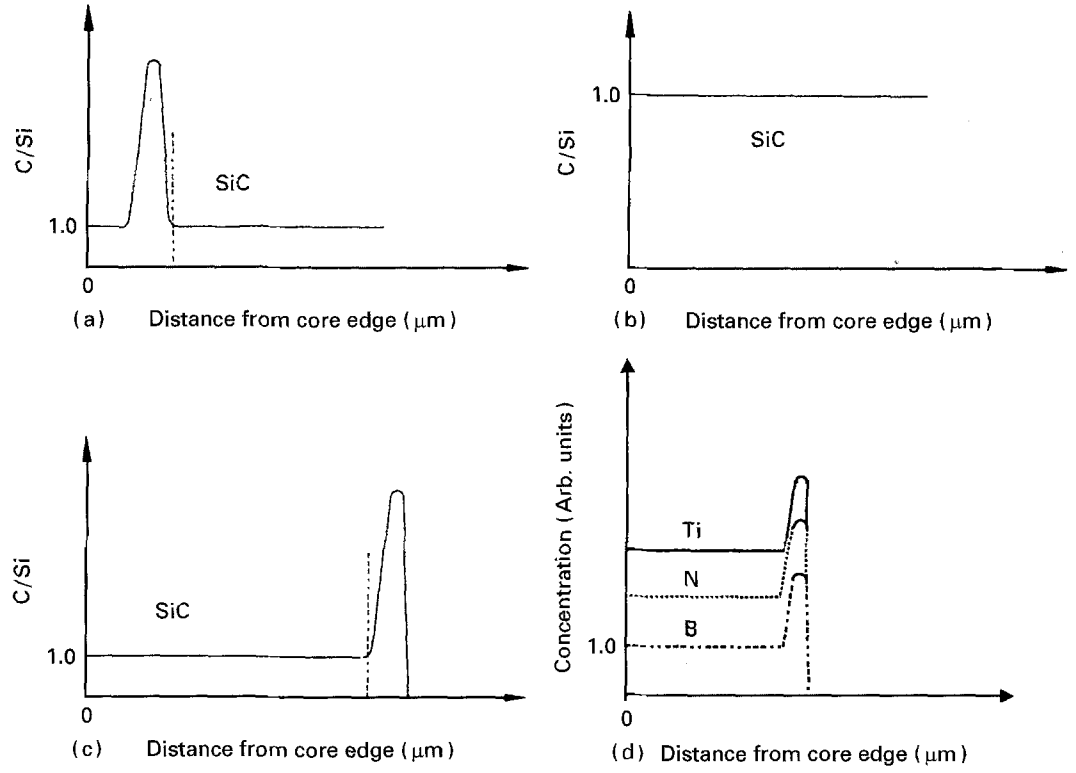

Figure 4 Schematic X-ray (WDX) linescans of SiC fibres: (a) SAM1, (b) SAM2, (c) Sigma SM1140, and (d) outermost coating of SAM1 fibre.

Another interesting observation in Fig. 2 is the difference in SiC grain size near to the core. The SiC grain size depends on the deposition temperature and large grains are typical of depositions of SiC by CVD at high temperatures [19]. In SAM1 fibre, the SiC grains size within the SiC coating region seems to be smaller than in the main SiC deposit. Both the SiC and carbon coatings may have been deposited at low temperature to achieve a small SiC grain size followed by the main SiC deposition in the second stage of the CVD reactor. The SiC grain size near to the tungsten core in the Sigma fibre is approximately 100–200 nm while in the SCS series fibre it is between 50 and 150 nm [6, 20]. In the case of Sigma fibre, the SiC grains become progressively finer towards the outer surface [9]. In contrast to Sigma fibres, the SCS series fibres have a distinct mid-radial boundary. A sudden change in the concentration of the deposition gases during SiC deposition on a carbon substrate may have resulted in the deposition of finer SiC grains and hence, a mid-radial boundary [5].

Fig. 6a–f shows a schematic drawing of each SiC fibre. The SAM2 fibre has an unusually large diameter of approximately 170 μm. The CVD deposition of SiC to such a large diameter on a 20 μm tungsten substrate may result in degradation of fibre strength. Again, it was not possible to determine the exact purpose of such a large diameter due to the limited amount of fibres available for tensile testing. Both the silicon and carbon concentrations do not vary across the fibre

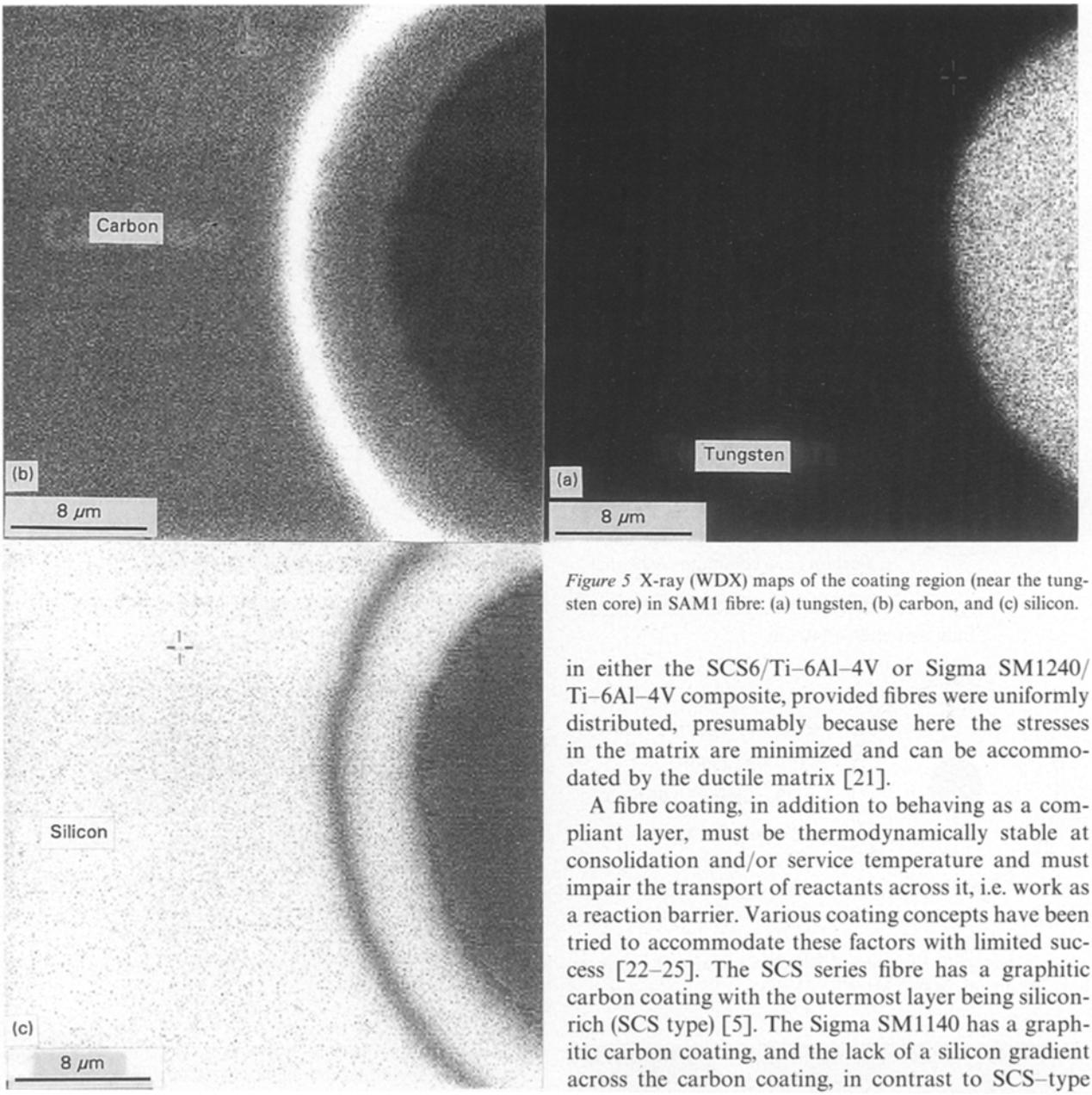

Figure 5 X-ray (WDX) maps of the coating region (near the tungsten core) in SAM1 fibre: (a) tungsten, (b) carbon, and (c) silicon.

radius (Fig. 4b) and the absence of SiC and carbon coatings on the tungsten core (as is the case with SAM1 fibre) is clear in Fig. 1b.

3.2. Description of the fibre coatings

A fibre coating serves three purposes: (a) to minimize handling damage, (b) to act as a compliant layer to accommodate the coefficient of thermal expansion (CTE) mismatch between the SiC fibre and metal matrix, and (c) to control chemical interaction. For example, Fig. 7 shows the presence of thermal stress-induced cracking of both the matrix and the fibre coating after consolidation during "cool-down" in a SCS6/TiAl composite. It suggests that the coating on the SCS6 fibre is not always an effective compliant layer for preventing the thermal stress-induced cracking. The presence of thermal stress-induced cracking of the matrix was observed also in Sigma SM1240 fibre-reinforced TiAl [20]. No cracking was observed in either the SCS6/Ti–6Al–4V or Sigma SM1240/Ti–6Al–4V composite, provided fibres were uniformly distributed, presumably because here the stresses in the matrix are minimized and can be accommodated by the ductile matrix [21].

A fibre coating, in addition to behaving as a compliant layer, must be thermodynamically stable at consolidation and/or service temperature and must impair the transport of reactants across it, i.e. work as a reaction barrier. Various coating concepts have been tried to accommodate these factors with limited success [22–25]. The SCS series fibre has a graphitic carbon coating with the outermost layer being silicon-rich (SCS type) [5]. The Sigma SM1140 has a graphitic carbon coating, and the lack of a silicon gradient across the carbon coating, in contrast to SCS–type coating, is clear in the schematic X-ray (WDX) line-scan as seen in Fig. 4c. The Sigma SM1240 has a duplex-type of coating of partially turbostratic carbon (adjacent to SiC) and TiB_x on the surface [26, 27]. The SCS0 and SAM2 fibres are uncoated.

The SAM1 fibre has a coating consisting of a compound(s) of titanium, boron and nitrogen as seen in Fig. 4d. However, the deposition process is not known. It is possible that a sputtering method was used involving deposition of TiB_2 in the nitrogen environment. Another possibility is that TiB_2 was deposited using chemical or physical vapour deposition processes followed by heating in a nitrogen environment.

3.3. Qualitative assessment of oxygen in SiC fibres

Table II shows the mean of the C/Si and Si/O ratios determined from the Auger spectra for each fibre. The C/Si ratio for each fibre is within 1.5 ± 0.15, indicating the consistency of Auger analysis. Furthermore, it suggests that carbon contamination (if occurring)

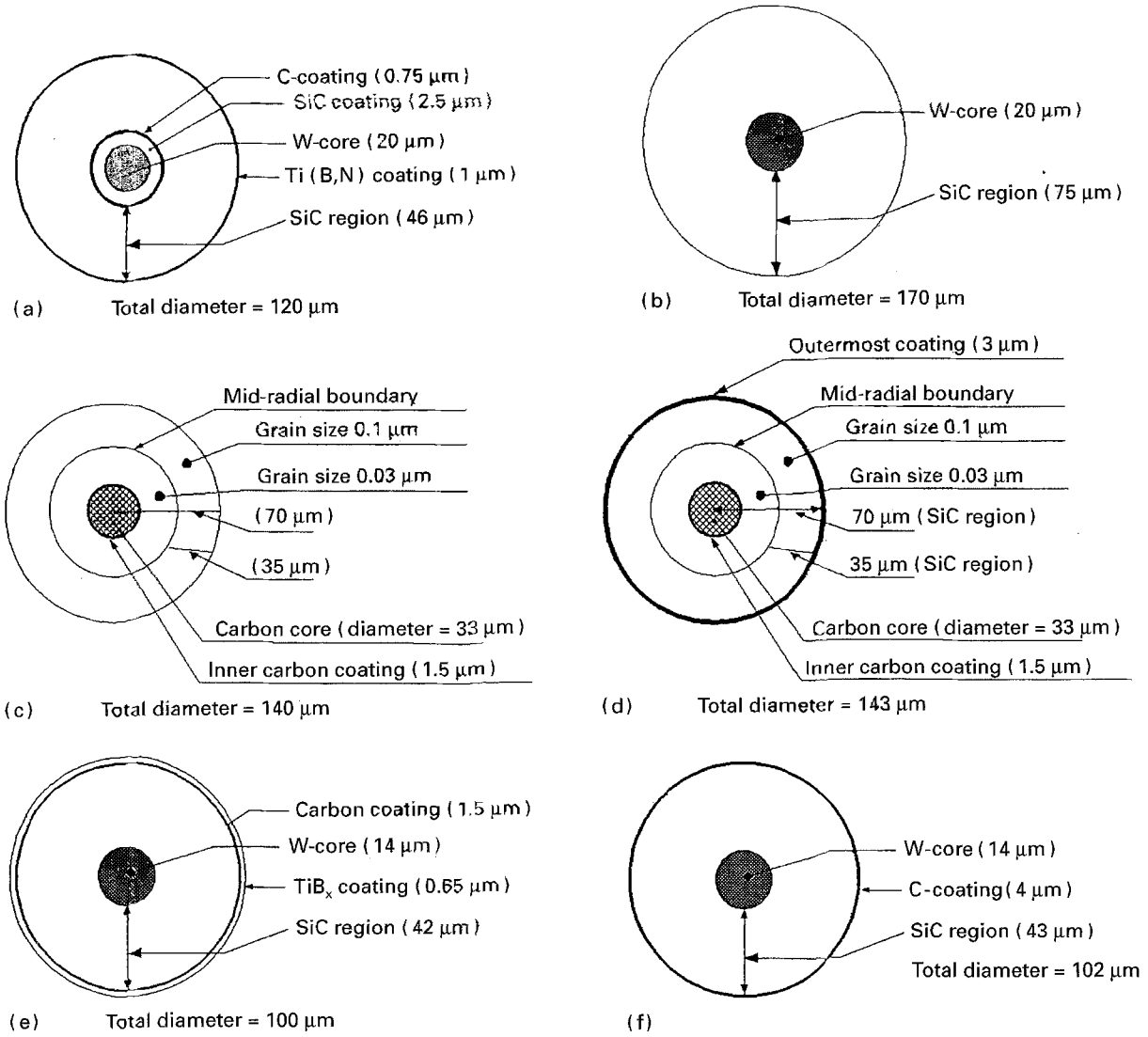

Figure 6 Schematic diagrams of SiC fibres showing the thickness of various layers: (a) SAM1, (b) SAM2, (c) SCS0, (d) SCS6, (e) Sigma SM1240, and (f) Sigma SM1140.

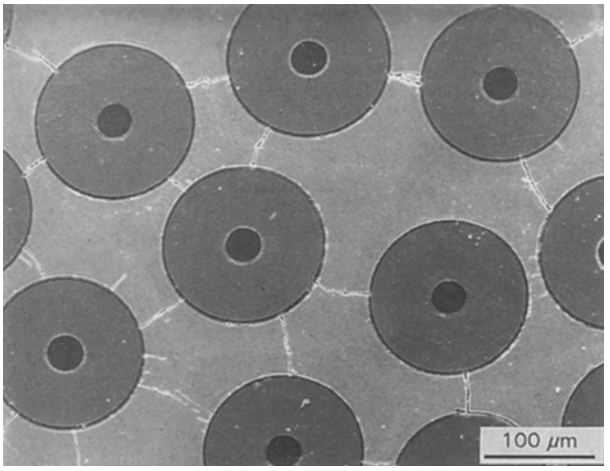

Figure 7 Scanning electron micrograph of SCS6/TiAl composite, showing extensive thermal stress-induced cracking of the fibre coating and the matrix; specimens were consolidated at 1173 K/150 MPa/2 h using hot isostatic pressing.

during analysis is uniform for each fibre. This Auger spectrometer is routinely used for the study of the fracture surfaces of aluminium alloys using the procedure adopted in this study [28]. No evidence of *in situ* oxidation and/or contamination of the fracture surfaces was observed thus ensuring to a high degree of confidence that the presence of oxygen recorded in this study is, indeed, a result of variations in process parameters and production methods of the candidate fibres. Fig. 8 shows the sample Auger spectrum taken from the centre of the main SiC region of each fibre.

Silicon, carbon and oxygen yields ("yield" in the present context means net Auger peak intensity determined from the Auger point spectra using a peak-background algorithm) were determined for each fibre

TABLE II Mean of C/Si and Si/O ratios as determined from Auger point spectra taken from *in situ* fractured fibres

Fibre	Mean C/Si	Mean Si/O	Si*/O[a]
SAM1 (main SiC region)	1.44	2.31	2.14
SAM1 (SiC coating)	1.30	3.50	3.11
SAM2	1.71	1.72	1.90
SCS0	1.37	4.22	3.81
SCS6	1.68	1.76	2.14
Sigma (SM1240)	1.33	2.25	2.14

[a] In order to eliminate the effect of varying silicon yield, data in column 4 (Si*/O) are calculated using an average silicon yield for all the fibres and divided by oxygen yield for each fibre.

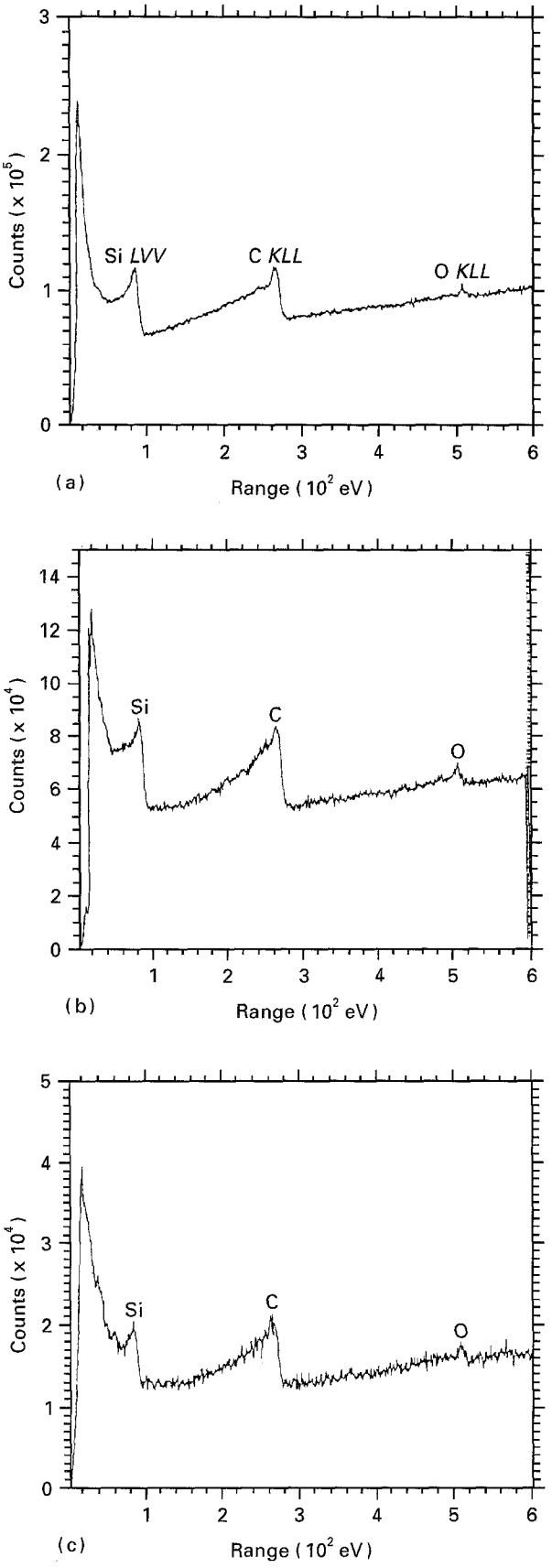

Figure 8 Typical sample of Auger electron spectroscopy (AES) point spectra from the main SiC deposition region of (a) SCS0, (b) SCS6, (c) SAM1, (d) SAM, and (e) Sigma SM1240.

and are shown in Table III. The carbon Auger yield was approximately the same for each fibre suggesting carbon contamination was not occurring and had no effects on the results. The silicon yield was also constant except for the SAM2 and SCS6 fibres. A decrease in silicon yield for SAM2 and SCS6 fibres is accounted for by an increase in the oxygen yield. However, there was a difference in the silicon yield for SCS0 and SCS6 even though the SiC region of both the fibres was essentially the same. This difference is probably associated with the Auger spectrum taken from different parts of the main SiC region. For SCS series fibres, silicon concentration varied across the fibre diameter and increased towards the outer edge [5]. Differences in topographical features of the fractured fibre surfaces may have affected the silicon yield. However, carbon yield for both the SCS0 and SCS6 fibres were the same. The oxygen yield lay between 0.9 (SCS0) and 0.18 (SAM2). The data suggest that the oxygen yield varied from fibre to fibre with the SCS0 having less oxygen than the other SiC fibres. Research is underway to determine the significance of the differences in the oxygen yield between the various fibres i.e. to quantify the amount of oxygen in each fibre.

Table II shows the mean Si/O ratio for each fibre. A small change in silicon yield will have a pronounced effect on the Si/O ratio, probably resulting from the topographical effects. To eliminate the effect of varying silicon yield, an average silicon yield, Si*, (Si* = 0.3425) was determined for every fibre. Table II shows Si*/O ratios (column 4). The SCS0 fibre has the

TABLE III Qualitative assessment of oxygen for different continuous silicon carbide fibres showing silicon, carbon, and oxygen yields as determined from Auger point spectra taken from *in situ* fractured fibres

Sic fibre	No. of fibres fractured	$\frac{I_{SiLVV}}{I_{SiLVV}+I_{CKLL}+I_{OKLL}}$ [a]	$\frac{I_{CKLL}}{I_{SiLVV}+I_{CKLL}+I_{OKLL}}$	$\frac{I_{OKLL}}{I_{SiLVV}+I_{CKLL}+I_{OKLL}}$
SAM1 (SiC region)	4	0.340 ± 0.06 (8)[b]	0.490 ± 0.08 (8)	0.160 ± 0.06 (8)
SAM1 (SiC coating)	2	0.385 (2)	0.50 (2)	0.110 (2)
SAM2	7	0.310 ± 0.11 (7)	0.530 ± 0.08 (7)	0.180 ± 0.15 (7)
SCS0	8	0.38 ± 0.10 (14)	0.52 ± 0.09 (14)	0.09 ± 0.03 (14)
SCS6	5	0.280 ± 0.10 (9)	0.550 ± 0.14 (9)	0.160 ± 0.04 (9)
Sigma SM1240	8	0.360 ± 0.14 (13)	0.480 ± 0.14 (13)	0.16 ± 0.08 (13)

[a] *LVV*, *KLL* = X-ray nomenclature.
[b] Mean yield ± standard deviation (numbers of AES spectra evaluated).

highest Si*/O ratio and thereby qualitatively the least oxygen compared to the other SiC fibres. Furthermore, SCS6, Sigma SM1240, SAM1 fibres have similar Si*/O ratios, suggesting similar oxygen levels. The SAM2 fibre has the highest oxygen yield.

4. Conclusions

Two types of SiC fibres (SAM1 and SAM2) produced in the Ukraine (former USSR) were analysed together with Sigma SM1240, Sigma SM1140, and SCS series (SCS0 and SCS6) fibres. Qualitative assessment of oxygen was performed for each SiC fibre. The uncoated SCS0 fibre had the least oxygen compared to SiC fibres produced in the former USSR, SCS6, and Sigma SM1240 fibres. The SAM1 fibre has a duplex SiC and carbon coating deposited over tungsten substrate prior to the main SiC deposition, to decouple mechanically the tungsten core from the main SiC region. The outermost coating on SAM1 fibre consists of a compound(s) of titanium, boron and nitrogen. The SAM2 fibre has a large (170 μm) diameter and is uncoated.

Acknowledgements

The authors thank Professor J. E. Castle for the provision of research facilities at the Department of Materials Science and Engineering, University of Surrey, Guildford, UK, and also Ms Li Sun for her help in operating the Auger Spectrometer. This work was carried out at the University of Surrey under a Memorandum of Understanding (MOU) between the University of Surrey and the University of Idaho.

References

1. P. R. SMITH and F. H. FROES, *J. Metals* **36**(3) (1984) 19.
2. W. A. ZDANIEWSKI and H. P. KIRCHNER, *J. Am. Ceram. Soc.* **70** (1987) 548.
3. E. A. GULBRANSEN, K. F. ANDREW and F. A. BRASSART, *J. Electrochem. Soc.* **113** (1966) 1311.
4. A. G. TURNBULL and M. W. WADEY, "CSIRO Thermochemistry System, Version V", Institute of Mineral, Energy and Construction, Port Melbourne, Victoria, Australia (1993).
5. F. E. WAWNER, in "Fiber reinforcement for composite materials", Composite Materials Series, edited by A. R. Bunsell, Vol. 2 (Elsevier, 1988) pp. 371–425.
6. X. J. NING and P. PIROUZ *J. Mater. Res.* **6** (1991) 2234.
7. S. R. NUTT and F. E. WAWNER, *J. Mater. Sci.* **20** (1985) 1953.
8. F. E. WAWNER, A. Y. TENG and S. R. NUTT, *SAMPE Q.* April (1983) 39.
9. D. IMESON and A. H. GRACE, "BP Metal Composites", Sunbury, UK Report 138141 (1992).
10. A. M. RITTER, F. CLARK and P. DUPREE, in "Light weight alloys for aerospace applications", edited by E. W. Lee and N. J. Kim (TMS, Warrendale, PA, 1991) pp. 403–12.
11. G. DAS, *Metall. Trans.* **21A** (1990) 1571.
12. W. WEI, *J. Mater. Sci.* **27** (1992) 1801.
13. *Idem*, in "Fundamental relationships between microstructure and mechanical properties of metal matrix composites", edited by P. K. Liaw and M. N. Gungor (AIME, Warrendale, PA, 1990) pp. 353–60.
14. J. D. CASEY and J. D. GELLER, Research Report, Textron Speciality Materials, Lowell, MA (1992).
15. H. DEBOLT and T. HENZE, US Pat. 4068037, January 1978.
16. D. MARTINEAU, P. MARTINEAU, M. LAHAYE, R. PAILLER, R. NASLAIN, M. COUZI and F. CREUGE, *J. Mater. Sci.* **19** (1984) 2731.
17. D. UPADHYAYA, C. M. WARD-CLOSE, P. TSAKIROPOULOS and F. H. FROES, *Mater. Sci. Technol.* **10** (1994) 887.
18. R. A. SHATWELL, private communications, DRA Sigma, RAE Farnborough, UK (1993).
19. L. M. IVANOVA and A. A. PLETYUSHKIN, in "Silicon carbide", research report, edited by I. N. Frantsevich, translated from Russian by Simon Lyse (Consultants Bureau, NY, 1970) pp. 116–21.
20. D. UPADHYAYA and F. H. FROES, unpublished research (1994).
21. R. A. MACKAY, *Scripta Metall. Mater.* **167** (1990) 167.
22. F. E. WAWNER and D. B. GUNDEL, *SAMPE Q.* **23** April (1992) 13.
23. R. R. KIESCHKE, R. E. SOMEKH and T. W. CLYNE, *Acta. Metall. Mater.* **39** (1992) 427.
24. C. M. WARWICK, R. R. KIESCHKE and T. W. CLYNE, *ibid.* **39** (1992) 437.
25. S. M. JENG and J. M. YANG, *J. Mater. Res.* **8** (1993) 905.
26. D. UPADHYAYA, R. BRYDSON, C. M. WARD-CLOSE, P. TSAKIROPOULOS and F. H. FROES, *Mater. Sci. Technol.* **10** (1994) 797.
27. Z. X. GUO, B. DERBY and B. CANTER, *J. Microsc.* **169** (1993) 279.
28. M. A. BAKER and P. TSAKIROPOULOS, *Surf. Interface. Anal.* **20** (1993) 589.

Received 16 September 1994
and accepted 3 February 1995